LAWRENCE
LIVERMORE
NATIONAL
LABORATORY

LLNL-JRNL-831850

Optimization of high energy x ray production through laser plasma interaction

S. Le Pape, L. Divol, A. MacPhee, J. McNaney, M. Hohenberger, D. H. Froula, V. Glebov, O. Landen, C. Stoeckl, E. L. Dewald, S. Khan, C. Yeamans, P. Michel, M. Schneider, J. Knauer, J. Kilkenny, A. Mackinnon

February 16, 2022

High Energy Density Physics

Disclaimer

High Energy Density Physics 31 (2019) 13–18

Contents lists available at ScienceDirect

High Energy Density Physics

journal homepage: www.elsevier.com/locate/hedp

Optimization of high energy x ray production through laser plasma interaction

S. Le Pape*[,a], L. Divol[a], A. Macphee[a], J. McNaney[a], M. Hohenberger[b], D. Froula[b], V. Glebov[b], O.L. Landen[a], C. Stoeckl[b], E. Dewald[a], S. Khan[a], C. Yeamans[a], P. Michel[a], M. Schneider[a], J. Knauer[b], J. Kilkenny[c], A.J. Mackinnon[a]

[a] Lawrence Livermore National Laboratory, Livermore, CA 94550, USA
[b] Laboratory for Laser Energetics, University of Rochester, Rochester, NY 14636, USA
[c] General Atomics, San Diego, CA 92186, USA

ARTICLE INFO

Keywords:
High energy X-ray source
X ray radiography
Backlighter

ABSTRACT

A standard technique for generating a burst of hard x rays (above 30 keV) is to use ultra high intensity lasers incident on a target. The strong laser field causes rapid electron oscillations which then generate hard x rays via bremsstrahlung. We have demonstrated a new technique for optimizing the conversion efficiency of laser light to hard x rays at moderate $I\lambda^2$ (mid 10^{13} W/cm^2.μm^2) assuming that the two plasmon decay plasma instability is the predominant acceleration mechanism. In this scheme, electrons are not directly accelerated by the laser field but by electron plasma waves. Experiments at the National Ignition Facility show the effect of a pre-pulse on the hard x ray spectrum and conversion efficiency. Different experimental configurations are investigated to optimize the conversion efficiency using various pre-pulse levels as well as different target designs (gold vs. silver, varying target thickness, presence of an ablator layer of CH). The conversion efficiency of laser energy into photon above 30 keV for a 100 ps short pulse scales as $\sim I^{1.23}$ for laser intensity ranging from 1×10^{16} to 1×10^{17} W/cm^2 at 3ω for high Z target. A 1-ns-long pre-pulse pre-seeding an 88-ps Gaussian laser pulse coupled with a CH-coated thin Au target led the highest conversion efficiency above 30 keV of $\sim 3 \times 10^{-4}$.

1. Introduction

The generation of a bright x ray source above 30 keV to probe mid Z-elements at high pressure to study material strength [1,2] or high $\rho \times r$ capsule implosions [3] in the Inertial Confinement Fusion (ICF) context required so far the use of a high intensity laser (with peak intensity $> 10^{17}$ W/cm^2). In this regime, electrons are directly accelerated by the laser to temperature following the ponderomotive scaling [4], implying that lower laser intensity ($< 10^{16}$ W/cm^2) would not produce the hot electrons population required for hard x ray generation. In this paper, we report on the development of a hard x ray source at moderate laser intensity (mid 10^{15} W/cm^2) based on electron acceleration via the Two Plasmon Decay instability [5]. We have investigated the production of x rays above 30 keV over two orders of magnitude in $I\lambda^2$, from 10^{14} W.μm^2/cm^2 to 10^{16} W.μm^2/cm^2. Over this range of $I\lambda^2$, laser absorption transitions from inverse Bremsstrahlung [6] (about 10^{14} W.μm^2/cm^2) to resonant absorption up to 5×10^{15} W.μm^2/cm^2 [7]. To produce enough hot electrons to generate x rays above 30 keV at intensities where direct acceleration of electron is not the dominant process, we relied on the two plasmon decay instability (TPD) to generate energetic electrons. This new scheme will allow the development of large area backlighter used for radiography or long duration (several hundreds of picosecondes) to study the hydrodynamic evolution of a system at photon energy above 30 keV at moderate laser intensities.

The Two Plasmon Decay (TPD) instability is generally a significant risk in ICF, where hot electrons can preheat the fuel and degrade the implosion. As a result most studies have been focused on mitigating the TPD instability. Few experiments have tried to take advantage of the generation of high-energy electrons at moderate intensities. A recent exception is shock ignition, where hot electrons generated by TPD help drive a strong convergent shock [8]. In this study, we take advantage of the low TPD instability threshold to generate high-energy electrons in a regime where vacuum heating or resonant absorption are not the dominant processes. Experiments were performed on the National Ignition Facility (NIF) at Lawrence Livermore National Laboratory. The

* Corresponding author.
E-mail address: lepape2@llnl.gov (S. Le Pape).

https://doi.org/10.1016/j.hedp.2019.01.002
Received 19 September 2018; Received in revised form 19 November 2018; Accepted 10 January 2019
Available online 02 February 2019
1574-1818/

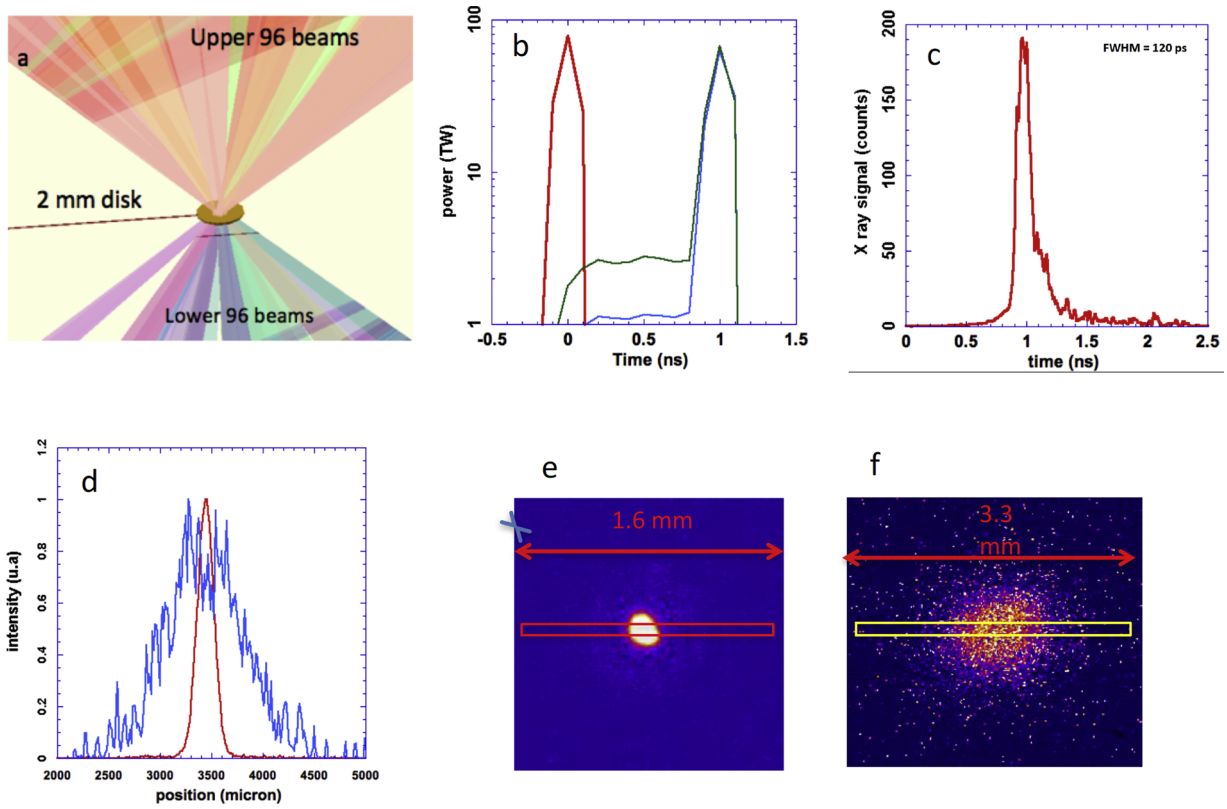

Fig. 1. (a) NIF experimental set up, silver targets are 25 μm thick, gold targets are 10 μm thick. (b) NIF laser pulse shape without pre-pule and with pre-pulse, red pulse is the 88 ps Gaussian pulse, blue and green pulse shapes are pulse shape with 1% and 5% pre-pulse. (c) X ray temporal profile measured with an X-ray streak camera (spider) on the NIF centered on 25 keV with a Full Width at Maximum of 2 keV. (d) Lineouts over X ray pinhole images of laser focal without phase plate (red) with phase plate (blue) in the 3 to 5 keV X-ray range. (e) Static X-ray images of laser focal spot without phase plate in the 3 to 5 keV X-ray range at 5×10^{15} W/cm^2, (f) with phase plate at 9×10^{16} W/cm^2. Rectangular area is the area where the line-outs display on figure d are made.

high-energy electron spectrum was optimized by varying target design and laser pulse shape. High-energy x ray yield above 30 keV was measured using a 5 mm-thick diamond CVD, x ray spectra were measured using a suite of calibrated x ray diodes. To optimize hot-electron production by TPD, as the TPD gain is linear with density scale length, high-Z targets (gold or silver) were coated with plastic (CH) and/or used a laser pulse shape with a pre-pulse. The generation of an underdense plasma to increase laser conversion efficiency into x rays already has been demonstrated [9–15]. These experiments were focused on increasing x-ray emission from thermal lines emitted in the hot coronal plasma, not on tailoring the high-energy part of the x-ray energy spectrum.

2. Experimental techniques and measurements

2.1. NIF experiments

The National Ignition Facility is a 192-beam laser system producing 1.8 MJ at 3ω [16]. Experiments reported in this paper used 96 NIF beams focused on a single point on each side of a high-Z disk placed at the center of the NIF target chamber (Fig. 1a). A 1-ns square pulse shape delivered by 4 beams on each side of the target forms the pre-pulse part of the pulse designed to create the initial plasma scale length. A 88 ps gaussian pulse directly following the end of the square pulse up to 100 J per beam forms the main pulse (Fig. 1b). The intensity on target was varied over 2 orders of magnitude by changing the focal spot diameter focusing the laser beam with or without phase plates. With phase plates in the beampath, the focal spot has a 1.2 mm diameter at best focus. Without phase plates, the focal spot has a 120 μm diameter containing half of the laser energy (Fig. 2d–f). The size of the laser spot

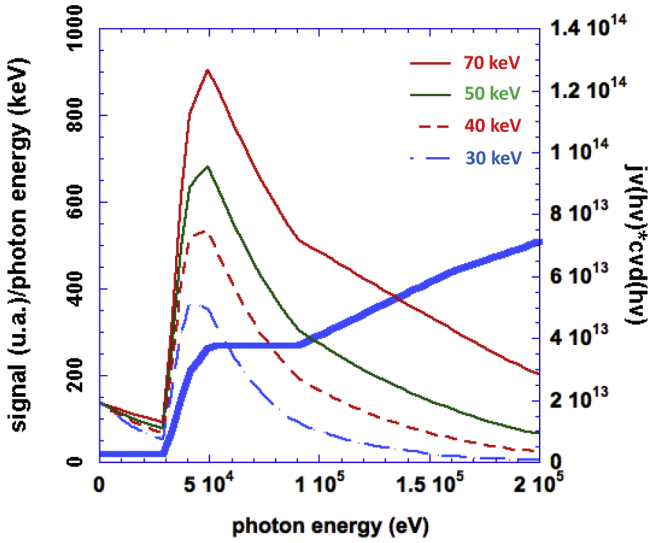

Fig. 2. Calculated CVD response and convolution of the spectrum with the CVD response as a function of photon energy for four hot electron temperatures 30, 40, 50 and 70 keV.The CVD response function was calculated using a Monte-Carlo code, its includes fluorescence and Compton electrons generated in the electrodes which deposit their energy in the diamond.

was checked on every shot using a time-integrated soft x-ray imager (SXI) [17] (Fig. 1 (d–f)).

A 5 mm thick CVD diamond detector was fielded to measure the x ray yield on every shot; it did sit behind a 4 mm aluminum filter cutting

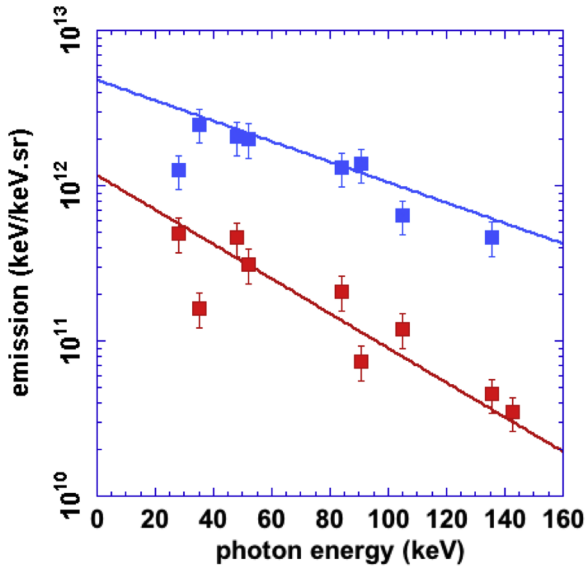

Fig. 3. X ray spectra measured by a suite of X-ray diodes (FFLEX). Squares are experimental data, curves are associated fits. These fits are used to infer the conversion efficiency of laser light into photons above 30 keV. Blue points and curve are a shot on a CH-coated gold target with a 5% pre-pulse without phase plate 5×10^{15} W/cm^2, red points and curve are a shot on a bare gold target using a 88 ps gaussian pulse without phase plate at 5×10^{15} W/cm^2.

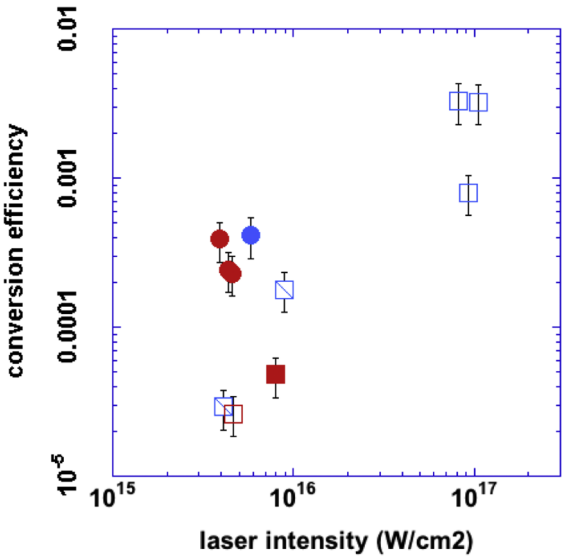

Fig. 4. Conversion efficiency of laser energy into photon above 30 keV inferred from FFLEX data. Red is gold target, blue is silver. Square are shot without pre-pulse, dots are shots with pre-pulse. solid dots or square are targets coated with CH.

most of the x rays bellow 30 keV (Fig. 2) [18,19]. X rays incident on the diamond generated electron-hole pair initiated by photoelectric events [20]. The diamond detector is placed in an aluminum well in a Diagnostic Instrument Manipulator (DIM). The aluminum from the well and the DIM shields the CVD electronic from x rays. Hot electrons were too slow to affect the measurement. The solid angle sustained by the CDV diamond on NIF is $\sim 5.9 \times 10^{-7} sr$, the detector angle to the target is 25°. Due to the random nature of hot electron trajectory in solid matter, X-ray bremsstrahlung emission is isotropic. Hot electrons accelerated by plasma waves are accelerated in the under-dense plasma at the position of the quarter critical surface then propagates to the solid density part of the target where bremsstrahlung emission takes place. The target thickness either 10 μm of gold or 25 μm of silver is lower or in the order of the attenuation length of 30 keV x rays (lower bound of the X-ray spectrum of interest in this paper) in solid cold matter meaning that the angle subtended by the detector does not impact significantly the measurement.

High-energy x ray spectra were recorded using the absolutely calibrated filter-fluorescer diagnostic (FFLEX) [21] (Fig. 3). A hot-electron population is then inferred from the measured hard x ray spectra. An exponentially falling hard x ray spectrum with a one temperature component following

$$I\left(\frac{keV}{keV \cdot sr}\right) = \frac{5e11}{4 \times \pi} \times \frac{Z^*}{47} * Ehot * exp\left(1 - \frac{h\nu}{thot}\right)$$

is assumed, where Ehot is the hot electron energy, and thot is the hot electron temperature [22,23]. This is used to calculate the expected signal on the ith FFLEX channel for a given hot-electron population. By comparing the predicted signal to the experimental data, the hot-electron temperature and energy content are determined through an iterative fitting process and a ξ^2 minimization analysis.

X ray temporal shape was recorded using a streak camera (SPIDER) on a 3-ns time window with 19-ps time resolution [24] (Fig. 1-c). The SPIDER photocathode is positioned behind four mid-Z filters, 11 μm Ge, 20 μm V, 8 μm Cu, and 5 μm Zr. Targets were high-Z silver or gold disks coated with a 10 μm CH layer.

3. Results

The NIF data are compiled in Fig. 4, which shows the conversion efficiency as a function of laser intensity, target design and pulse shape. The first clear observable trend is that the production of high energy photon scales with laser intensity (square on Fig. 4). It drops from 0.003 ± 0.0005at $\sim 10^{17}$ W/cm^2 to $3 \times 10^{-5} \pm 4 \times 10^{-6}$ at $\sim 5 \times 10^{15}$ W/cm^2 for the same target (bare silver), same pulse shape (88 ps gaussian pulse shape). These conversion efficiencies are in agreement with previous works [25] carried out on the Omega EP laser facility using a 100 ps laser pulse at 3ω. The second clear observable is the effect of the pre-pulse on CH-coated target on the production of hard x rays (solid dots on Fig. 4). For a silver target, adding the pre-pulse on the CH-coated target increases the conversion efficiency from $3 \times 10^{-5} \pm 4 \times 10^{-6}$ on bare silver to $4 \times 10^{-4} \pm 6 \times 10^{-5}$. Higher conversion efficiency might have been reached using larger than 10% pre-pulse level,but one of the constraint was to keep the temporal profile of the x ray pulse as short and sharp on the leading edge as possible. Fig. 2c shows the x ray temporal profile measured by a fast x ray streak camera for a 5% pre-pulse. Higher pre-pulse led to distortion of the rising edge of the pulse due to x-ray emission of the pre-formed plasma. Changing the target material from silver to gold without pre-pulse led to similar conversion efficiency $\sim 2.5 \times 10^{-5}$, and similar conversion efficiency level $\sim 4 \times 10^{-4}$ with pre-pulse for a CH-coated gold target versus silver. In conclusion, at similar laser intensity, adding the pre-pulse to the laser pulse and the CH-coating on the silver target resulted in an $\sim 14x$ increase of the conversion efficiency into photon above 30 keV. The effect of pre-pulse level is shown on Fig. 5a. Increasing the pre-pulse level from 0 to 5% (i.e 2.8TW) resulted in a boost of the conversion efficiency from $\sim 5 \times 10^{-5}$ to $\sim 4 \times 10^{-4}$. The hot electron temperature (Fig. 5-b) increased from ~ 40 keV without pre-pulse to ~ 90 keV at a 5% pre-pulse level.

Fig. 6shows the conversion efficiency as a function of laser intensity only for a bare silver target. A least-square fit to the data gives. CE $\sim 2 \times 10^{-3} \times I^{1.23}$ where I is the laser intensity divided by $1 \times 10^{16} \times \lambda^2$.

3.1. Simulation and discussion

We note a clear dependence of hot-electron temperature (Thot) with laser intensity. As the laser intensity increases, the temperature of

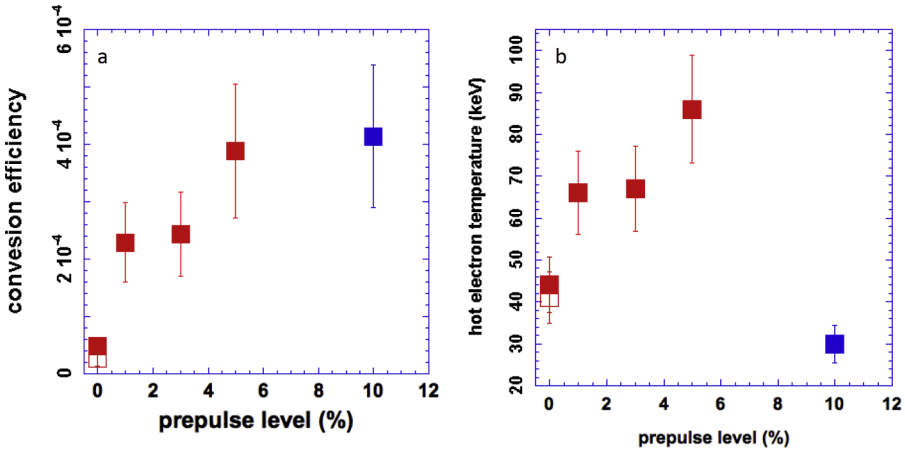

Fig. 5. (a) Conversion efficiency of laser energy into photons above 30 keV on gold target and silver targets inferred from FFLEX data. (b) Corresponding hot electron temperature inferred from FFLEX data. Empty square is bare gold target with phase plate, solid squares are CH-coated gold target with phase plate.- blue square is CH coated silver target with phase plate.

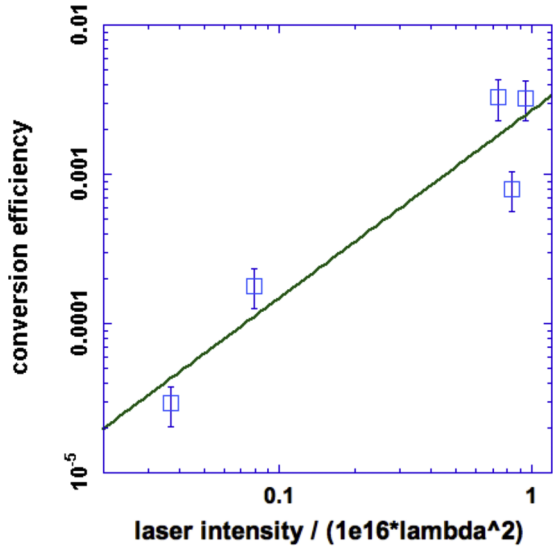

Fig. 6. Conversion efficiency of laser energy into photon above 30 keV inferred from FFLEX data for bare silver target on the NIF.

energetic electrons produced increases; high-energy x ray production also increases accordingly (Fig. 5). For short-pulse lasers at laser intensities ranging from 10^{19} W/cm^2 to low 10^{16} W/cm^2, the hot electron temperature follows the experimental Beg scaling [26] and analytical scaling [27]: $T_{hot}[keV] \approx 215 \times (I_{18} \times \lambda^2)^{1/3}$, where λ is in μm and I in W/cm^2. The absorption process consistent with these results is resonant absorption. The Beg scaling reproduces the trend observed on the 88 Gaussian pulse shots (squares on Fig. 4), implying that going to an intensity range of 5×10^{15} W/cm^2 at 3ω would result in a Thot ≈ 16 keV. The ponderomotive scaling [4], valid at higher $I\lambda^2$ would result in an even lower value of Thot as it scales as $\sqrt{(I\lambda^2)}$. In this regime (mid 10^{15} W/cm^2 at 3ω), with an imposed pre-pulse, the mechanism of electron acceleration is different from that dictated by the Beg scaling. Electrons with energies up to 100 keV can be generated through acceleration by Langmuir waves via the TPD instability. An extensive literature database, both experimental and theoretical, has been published on the TPD instability, primarily in the ICF context [28–31]. The linear gain of the TPD instability in the multibeam configuration with polarization smoothing is a function of plasma scale length and electron temperature and scales as:

$$\bar{G}_c = \frac{I^{14} \times L_n \times \lambda}{T_e}. \quad (1)$$

where I is the laser intensity in W/cm^2, L_n is the plasma scale length in μm, λ is the laser wave length in μm and T_e is the bulk electron temperature in keV.

The intensity and length of the pre-pulse has been designed to meet a few requirements (the energy and temporal profile of the Gaussian pulse is set by the laser capabilities): (1) create a sufficiently long plasma scale length to trigger the TPD instability. (2) Pre-plasma not to be long enough to absorb most of the laser light before reaching quarter critical, thus reducing the TPD gain. (3) Quarter critical surface does not stand too far from the high-Z layer to maximize high-energy electron to high-Z layer coupling. (4) Shock launched by the pre-pulse does not reach the back surface of the high-Z layer before the 88-ps Gaussian pulse arrives.

The hydrodynamic expansion of the target has been modeled using the 2D radiation hydrodynamic code HYDRA [32]. HYDRA output was then post-processed to calculate plasma scale lengths and TPD gains. Table 1 shows results of the HYDRA simulations for different levels of pre-pulse on a CH-coated silver target. Going from a non-pre-pulse case to a 4-kJ/ns pre-pulse, the plasma scale length changes from 20 to 300 μm and the TPD gain from about 1 to 15. The trend observed in simulation is similar to the trend observed experimentally (Fig. 6): a larger scale length leads to higher gain and increased high-energy emission.

The boost of Thot with the pre-pulse level (Fig. 5b) from 40 to 70 keV at 1% and up to 80 keV with a 5% pre-pulse level is also characteristic of TPD. As the gain rises, the hot electron temperature is predicted to linearly increase [33]. Increasing the pre-pulse level from 5% to 10% on a CH-coated silver target the spectrum content of the x ray emission changed. The lower part of the spectrum increased while the harder part went down, i.e the hot electron temperature went from 80 to 30 keV. Nevertheless total amount of hard x ray generated went up from 50 J to 200 J. Gain calculation shows that the TPD gain drops slightly going from 5% to 10% pre-pulse level because even if the plasma scale length grows, the plasma temperature is hotter (Table 1). Meanwhile, going from 5% to 10% results in an increase of a factor of 2 of stimulated Raman scattering (SRS) gain. This could explain the drop in electron temperature at the higher pre-pulse level, transitioning from TPD to SRS, but without information on the wavelength of the scattered light we cannot be more conclusive.

Table 1
Summary of plasma parameters with pre-pulse level from HYDRA simulation.

PP power (TW)	Ln[μm]	bulk Te [keV] at 1 ns	TPD gain at peak power
0.001 no PP	20	1	0.95
0.4 i.e 1% PP	160	1	7.6
1 i.e 2.5% PP	200	1.4	9.5
4 i.e 10% PP	300	3.5	14.2

3.2. Summary

We have presented a set of experimental data characterizing high-energy x ray emission at intensities ranging from mid-10^{15} W/cm^2 to 10^{17} W/cm^2 carried out at the NIF laser facilities (0.351-μm light). Emission was characterized using a CVD diamond, sensitive to above 30 keV x-rays, and FFLEX measuring the hard x ray spectra. The conversion efficiency of laser energy into photon above 30 keV for a 100 ps short pulse scales as $\sim I^{1.23}$ for laser intensity ranging from 1×10^{16} to 1×10^{17} at 3ω. Experimental data show a gain in conversion efficiency from laser light to hard x rays (> 30 keV) by a factor of 14 when a thin CH coating is added to the front of the high-Z target and a long (> 1 ns) low-power (5%) pre-pulse is added before the main 88-ps Gaussian pulse. These experimental data are consistent with acceleration of energetic electrons by plasma waves driven by the Two Plasmon Decay instability around quarter critical density. As the plasma scale length gets larger due to the low-Z coating and pre-pulse, the TPD gain grows and so does high-energy emission and hot-electron temperature. Experimental trends follow expectation of linear gain scalings derived from radiation hydrodynamic simulations and experimental data gathered in the context of direct-drive ICF studies. Increase on plasma scale length led to an increase of hard X-ray production due to TPD electrons. Our focus has been on developing a bright source of high energy at moderate intensities (mid-10^{15} W/cm^2) where the ponderomotive force is too weak to accelerate electrons to high enough energies. Using the electric field of plasma waves generated by laser-plasma instabilities instead has been proven successful. Experimental data show that the presence of a pre-pulse does increase the conversion efficiency without impacting the time history of hard x ray emission. This type of bright high energy x-ray source could be used for large areal backlighter experiments such as Compton radiography, where reaching a higher intensity (typically mid-10^{16} W/cm^2) would require a high-energy short-pulse laser system.

Acknowledgments

This work was performed under the auspices of the U.S. Department of Energy by Lawrence Livermore National Laboratory under Contract DE-AC52-07NA27344. Work was also supported by the Laboratory Directed Research and Development Grant 11-ERD-050 and the National Laboratory User Facility.

Appendix

A proof of concept campaign has been carried out on the Omega laser facility prior to the NIF campaign. On the Omega laser facility, 20 laser beams all focused at the same point using OMEGA E-IDI 300 DPP phase plate. the pulse shape was a PS100ps, a 100-ps full-width-half-maximum applied on all 20 beams with a maximum energy of 50 J per beam. On a subset of shots a pre-pulse was induced using 100 ps beams stacked in times up to 500 ps. Identical to NIF targets and CVD diamond detector were used on the Omega facility. During the Omega campaign, a few target and laser options were tested. The baseline shot, a bare silver flat foil was shot to connected to previous NIF data. On Omega adding a CH coating to a high Z foil did not result in an increased production of x ray, the laser did not ablated enough CH to produce a long enough plasma scale length. Adding the a pre-pulse did greatly increase the x ray signal production given time to the under-dense plasma to develop, by a factor of 4, measured by the cvd diamond. The hot electron temperature measured by the x ray diodes also increased from ~ 40-30 keV to ~ 70 keV. The increase of x ray production and hot electron temperature thanks to the addition of laser pre-pulse and low Z coating is in agreement with the experimental data obtained on the NIF (Fig. 7).

Laser intensity (W/cm2)	Target type	CVD signal (V)	Thot (keV)
1.3e16	Bare Silver	0.31	42
1.3e16	CH coated gold	0.09	30
9.4e15	CH coated silver with CH and pre pulse	1.32	72

Fig. 7. Table of experimental data from Omega shots.

References

[1] B.A. Remington, G. Bazan, J. Belak, E. Bringa, J.D. Colvin, M.J. Edwards, S.G. Glendinning, D.H. Kalantar, M. Kumar, B.F. Lasinski, K.T. Lorenz, J.M. McNaney, S.M. Pollaine, D. Rowley, J.S. Stölken, S.V. Weber, W.G. Wolfer, M. Caturla, D.S. Ivanov, L.V. Zhigilei, B. Kad, M.A. Meyers, M. Schneider, D.D. Meyerhofer, B. Yaakobi, J.S. Wark, High-resolution 17–75 keV backlighters for high energy density experiments, Phys. Plasmas 15 (7) (2008) 2587–2607.

[2] R. Tommasini, H.-S. Park, P. PATEL, B. Maddox, S. Le Pape, S.P. Hatchett, B.A. Remington, M.H. Key, N. Izumi, M. Tabak, Development of Compton radiography using high-Z backlighters produced by ultra-intense lasers, AIP Conf. Proc. 926 (2007) 248–258. (At. Processes Plasmas)

[3] J. Lindl, Development of the indirect-drive approach to inertial confinement fusion and the target physics basis for ignition and gain, Phys. Plasmas 2 (11) (1995) 3933–4024.

[4] S.C. Wilks, W.L. Kruer, M. Tabak, A.B. Langdon, Absorption of ultra-intense laser pulses, Phys. Rev. Lett. 69 (1992) 1383–1386, https://doi.org/10.1103/PhysRevLett.69.1383.

[5] H. Figueroa, C. Joshi, H. Azechi, N. Ebrahim, K. Estabrook, Stimulated raman scattering, two-plasmon decay, and hot electron generation from underdense plasmas at 0.35 μm, Phys. Fluids 27 (7) (1984) 1887–1896. (1958–1988)

[6] P. Gibbon, E. Förster, Short-pulse laser-plasma interactions, Plasma Phys. Control. Fusion 38 (6) (1996) 769–793.

[7] R. Fedosejevs, R. OTTMANN, R. Sigel, G. KUHNLE, S. SZATMARI, F.P. SCHAFER, Absorption of femtosecond laser-Pulses in high-density plasma, Phys. Rev. Lett. 64 (11) (1990) 1250–1253.

[8] V. Smalyuk, D. Shvarts, R. Betti, J. Delettrez, D. Edgell, V.Y. Glebov, V. Goncharov, R. McCrory, D. Meyerhofer, P. Radha, et al., Role of hot-electron preheating in the compression of direct-drive imploding targets with cryogenic d 2 ablators, Phys. Rev. Lett. 100 (18) (2008) 185005.

[9] F. Girard, J.P. Jadaud, M. Naudy, B. Villette, D. Babonneau, M. Primout, M.C. Miller, R.L. Kauffman, L.J. Suter, J. Grun, J. Davis, Multi-keV x-ray conversion efficiencies of laser-preexploded titanium foils, Phys. Plasmas 12 (9) (2005) 092705.

[10] C.A. Back, J. Grun, C. Decker, L.J. Suter, J. Davis, O.L. Landen, R. Wallace, W.W. Hsing, J.M. Laming, U. Feldman, M.C. Miller, C. Wuest, Efficient multi-keV underdense laser-produced plasma radiators, Phys. Rev. Lett. 87 (2001) 275003, https://doi.org/10.1103/PhysRevLett.87.275003.

[11] K.B. Fournier, J.H. Satcher, M.J. May, J.F. Poco, C.M. Sorce, J.D. Colvin, S.B. Hansen, S.A. MacLaren, S.J. Moon, J.F. Davis, F. Girard, B. Villette, M. Primout, D. Babonneau, C.A. Coverdale, D.E. Beutler, Absolute x-ray yields from laser-irradiated germanium-doped low-density aerogels, Phys. Plasmas 16 (5) (2009), https://doi.org/10.1063/1.3140041.

[12] M. Barrios, S. Regan, K. Fournier, R. Epstein, R. Smith, A. Lazicki, R. Rygg, D. Fratanduono, J. Eggert, H.-S. Park, et al., X-ray area backlighter development at

the national ignition facility (invited), Rev. Sci. Instrum. 85 (11) (2014) 11D502.
[13] L. Jacquet, M. Primout, B. Villette, F. Girard, G. Oudot, Comparison of x-ray source concepts for radiographic purposes at omega, High Energy Density Phys. 9 (3) (2013) 601–608.
[14] R. Kodama, T. Mochizuki, K. Tanaka, C. Yamanaka, Enhancement of keV x-ray emission in laser-produced plasmas by a weak prepulse laser, Appl. Phys. Lett. 50 (12) (1987) 720–722.
[15] L. Jarrott, A. Kemp, L. Divol, D. Mariscal, B. Westover, C. McGuffey, F. Beg, M. Suggit, C. Chen, D. Hey, et al., Kα and bremsstrahlung x-ray radiation backlighter sources from short pulse laser driven silver targets as a function of laser prepulse energy, Phys. Plasmas 21 (3) (2014) 031211. (1994-present)
[16] E.I. Moses, R.N. Boyd, B.A. Remington, C.J. Keane, R. Al-Ayat, The national ignition facility: ushering in a new age for high energy density science, Phys. Plasmas 16 (4) (2009), https://doi.org/10.1063/1.3116505.
[17] M.B. Schneider, O.S. Jones, N.B. Meezan, J.L. Milovich, R.P. Town, S.S. Alvarez, R.G. Beeler, D.K. Bradley, J.R. Celeste, S.N. Dixit, M.J. Edwards, M.J. Haugh, D.H. Kalantar, J.L. Kline, G.A. Kyrala, O.L. Landen, B.J. MacGowan, P. Michel, J.D. Moody, S.K. Oberhelman, K.W. Piston, M.J. Pivovaroff, L.J. Suter, A.T. Teruya, C.A. Thomas, S.P. Vernon, A.L. Warrick, K. Widmann, R.D. Wood, B.K. Young, Images of the laser entrance hole from the static x-ray imager at NIF, Rev. Sci. Instrum. 81 (10) (2010) 10E538.
[18] M.A. RUSSOTTO, R.L. KREMENS, Measurement of fuel ion temperatures in ICF implosions using current-Mode neutron time-of-flight detectors, Rev. Sci. Instrum. 61 (10) (1990) 3125–3127.
[19] V. Glebov, C. Stoeckl, T.C. Sangster, S. Roberts, G.J. Schmid, R.A. Lerche, M.J. Moran, Prototypes of national ignition facility neutron time-of-flight detectors tested on OMEGA, Rev. Sci. Instrum. 75 (10) (2004) 3559–3562.
[20] A. MacPhee, D. Edgell, E. Bond, D. Bradley, C. Brown, S. Burns, J. Celeste, C. Cerjan, M. Eckart, V. Glebov, et al., A diamond detector for x-ray bang-time measurement at the national ignition facility, J. Instrum. 6 (02) (2011) P02009.
[21] M. Hohenberger, F. Albert, N.E. Palmer, J.J. Lee, T. Doppner, L. Divol, E.L. Dewald, B. Bachmann, A.G. MacPhee, G. LaCaille, D.K. Bradley, C. Stoeckl, Time-resolved measurements of the hot-electron population in ignition-scale experiments on the national ignition facility (invited), Rev. Sci. Instrum. 85 (11) (2014) 11D501.
[22] K.A. Brueckner, Energy deposition in laser-heated plasmas, Phys. Rev. Lett. 36 (1976) 677–679, https://doi.org/10.1103/PhysRevLett.36.677.
[23] R.P. Drake, R.E. Turner, B.F. Lasinski, E.A. Williams, K. Estabrook, W.L. Kruer, E.M. Campbell, T.W. Johnston, X-ray emission caused by raman scattering in long-scale-length plasmas, Phys. Rev. A 40 (1989) 3219–3225, https://doi.org/10.1103/PhysRevA.40.3219.
[24] S. Khan, P. Bell, D. Bradley, S. Burns, J. Celeste, L. Dauffy, M. Eckart, M. Gerhard, C. Hagmann, D. Headley, et al., Measuring x-ray burn history with the streaked polar instrumentation for diagnosing energetic radiation (spider) at the national ignition facility (NIF), SPIE Optical Engineering + Applications, International Society for Optics and Photonics, 2012. 850505–850505.
[25] R. Tommasini, S. Hatchett, D. Hey, C. Iglesias, N. Izumi, J. Koch, O. Landen, A. MacKinnon, C. Sorce, J. Delettrez, et al., Development of Compton radiography of inertial confinement fusion implosions, Phys. Plasmas 18 (5) (2011) 056309. (1994-present)
[26] F.N. Beg, A.R. Bell, A.E. Dangor, C.N. Danson, A.P. Fews, M.E. Glinsky, B.A. Hammel, P. Lee, P.A. Norreys, M. Tatarakis, A study of picosecond laser-solid interactions up to 1019 W cm^{-2}, Phys. Plasmas 4 (2) (1997) 447–457, https://doi.org/10.1063/1.872103.
[27] M.G. Haines, M.S. Wei, F.N. Beg, R.B. Stephens, Hot-electron temperature and laser-light absorption in fast ignition, Phys. Rev. Lett. 102 (2009) 045008, https://doi.org/10.1103/PhysRevLett.102.045008.
[28] S.P. Regan, D.K. Bradley, A.V. Chirokikh, R.S. Craxton, D.D. Meyerhofer, W. Seka, R.W. Short, A. Simon, R.P.J. Town, B. Yaakobi, J.J.C. III, R.P. Drake, Laser-plasma interactions in long-scale-length plasmas under direct-drive national ignition facility conditions, Phys. Plasmas 6 (5) (1999) 2072–2080, https://doi.org/10.1063/1.873716.
[29] A. Simon, R.W. Short, E.A. Williams, T. Dewandre, On the inhomogeneous two-plasmon instability, Phys. Fluids 26 (10) (1983) 3107–3118, https://doi.org/10.1063/1.864037.
[30] J.F. Myatt, J. Zhang, J.A. Delettrez, A.V. Maximov, R.W. Short, W. Seka, D.H. Edgell, D.F. DuBois, D.A. Russell, H.X. Vu, The dynamics of hot-electron heating in direct-drive-implosion experiments caused by two-plasmon-decay instability, Phys. Plasmas 19 (2) (2012) 022707, https://doi.org/10.1063/1.3683004.
[31] D.H. Froula, B. Yaakobi, S.X. Hu, P.-Y. Chang, R.S. Craxton, D.H. Edgell, R. Follett, D.T. Michel, J.F. Myatt, W. Seka, R.W. Short, A. Solodov, C. Stoeckl, Saturation of the two-plasmon decay instability in long-scale-length plasmas relevant to direct-drive inertial confinement fusion, Phys. Rev. Lett. 108 (2012) 165003, https://doi.org/10.1103/PhysRevLett.108.165003.
[32] M.M. Marinak, G.D. Kerbel, N.A. Gentile, O. Jones, D. Munro, S. Pollaine, T.R. Dittrich, S.W. Haan, Three-dimensional hydra simulations of national ignition facility targets, Phys. Plasmas 8 (5) (2001) 2275–2280, https://doi.org/10.1063/1.1356740.
[33] S.X. Hu, D.T. Michel, D.H. Edgell, D.H. Froula, R.K. Follett, V.N. Goncharov, J.F. Myatt, S. Skupsky, B. Yaakobi, Hydrodynamic simulations of long-scale-length two-plasmon-decay experiments at the omega laser facility, Phys. Plasmas 20 (3) (2013), https://doi.org/10.1063/1.4794285.